Victor K. Lai
Department of Chemical Engineering
and Materials Science,
University of Minnesota – Twin Cities,
421 Washington Ave SE,
Minneapolis, MN 55455

Spencer P. Lake

Christina R. Frey

Department of Biomedical Engineering,
University of Minnesota – Twin Cities,
7-105 Nils Hasselmo Hall,
312 Church Street SE,
Minneapolis, MN 55455

Robert T. Tranquillo
Department of Chemical Engineering
and Materials Science,
University of Minnesota – Twin Cities,
421 Washington Ave SE,
Minneapolis, MN 55455;
Department of Biomedical Engineering,
University of Minnesota – Twin Cities,
7-105 Nils Hasselmo Hall,
312 Church Street SE,
Minneapolis, MN 55455

Victor H. Barocas[1]
Department of Biomedical Engineering,
University of Minnesota – Twin Cities,
7-105 Nils Hasselmo Hall,
312 Church Street SE,
Minneapolis, MN 55455
e-mail: baroc001@umn.edu.

Mechanical Behavior of Collagen-Fibrin Co-Gels Reflects Transition From Series to Parallel Interactions With Increasing Collagen Content

Fibrin and collagen, biopolymers occurring naturally in the body, are biomaterials commonly-used as scaffolds for tissue engineering. How collagen and fibrin interact to confer macroscopic mechanical properties in collagen-fibrin composite systems remains poorly understood. In this study, we formulated collagen-fibrin co-gels at different collagen-to-fibrin ratios to observe changes in the overall mechanical behavior and microstructure. A modeling framework of a two-network system was developed by modifying our micro-scale model, considering two forms of interaction between the networks: (a) two interpenetrating but noninteracting networks ("parallel"), and (b) a single network consisting of randomly alternating collagen and fibrin fibrils ("series"). Mechanical testing of our gels show that collagen-fibrin co-gels exhibit intermediate properties (UTS, strain at failure, tangent modulus) compared to those of pure collagen and fibrin. The comparison with model predictions show that the parallel and series model cases provide upper and lower bounds, respectively, for the experimental data, suggesting that a combination of such interactions exists between the collagen and fibrin in co-gels. A transition from the series model to the parallel model occurs with increasing collagen content, with the series model best describing predominantly fibrin co-gels, and the parallel model best describing predominantly collagen co-gels. [DOI: 10.1115/1.4005544]

Keywords: collagen, fibrin, microstructure, modeling, mechanical properties, tissue engineering

1 Introduction

Type I collagen and fibrin are important extracellular matrix proteins. Collagen I is the predominant load-bearing component in many tissues, such as skin and tendon, while fibrin provides mechanical strength and integrity in blood clots. In addition, these naturally occurring biopolymers are commonly used in tissue engineering applications [1–4] because of their biocompatibility and their ability to interact with cells and elicit functional cellular responses. In vivo, collagen and fibrin can be found together in granulation tissue during the wound healing process. In vitro, the co-existence of reconstituted collagen and fibrin matrices/fibril networks is seen in our tissue-engineered heart valve and media tissue equivalents (TEs), as the embedded cells gradually degrade the initial fibrin matrix and replace it with cell-derived collagen [5,6]. Separately, extensive work has been done on the mechanical properties of fibrin [7–12] and collagen I [13–17] matrices, however, there have been few studies on collagen-fibrin composite systems investigating how the two fibril networks interact to give the co-gel its macroscopic mechanical properties. Notable work includes that of Stegemann and co-workers [18–20], who observed that cell-seeded collagen-fibrin matrices exhibited a higher modulus but intermediate ultimate tensile stress compared to pure fibrin and pure collagen gels of the same overall protein concentration. However, the interpretation of these results is complicated by the inclusion of cells. Earlier efforts investigating possible interactions between collagen and fibrin networks include a study [21] that found evidence suggesting chemical cross-linking between collagen and fibrin via Factor XIII, a plasma enzyme that crosslinks fibrin. These findings, however, were refuted by others [22,23] who were unable to replicate the results. Thus, despite these considerable efforts, there remains an incomplete understanding of how collagen and fibrin fibril networks interact to confer overall mechanical properties. As tissue engineers strive to design tissues with mechanical properties comparable to native counterparts by creating multicomponent fiber networks (e.g., Ref. [18]), knowledge of such interactions is an important first step towards better understanding how multiple extracellular matrix (ECM) components influence the mechanical strength and stiffness of the overall tissue, allowing for more rational choices of scaffold components and culture conditions in the design. For example, in our fibrin-based TEs, an understanding of how the tissue stiffness changes with remodeling allows us to better predict the amount of compaction occurring in the tissues, which impacts overall fiber alignment, a factor that is crucial for conferring anisotropic mechanical properties akin to native tissues. In this study, we employ a combination of experimental and computational techniques to characterize and predict the mechanical behavior of

[1]Corresponding author: Victor H. Barocas, Department of Biomedical Engineering, University of Minnesota, 7-105 Nils Hasselmo Hall, 312 Church Street SE, Minneapolis, MN 55455.

Contributed by the Bioengineering Division of ASME for publication in the JOURNAL OF BIOMECHANICAL ENGINEERING. Manuscript received August 29, 2011; final manuscript received December 14, 2011; accepted manuscript posted January 23, 2012; published online February 8, 2012. Editor: Michael Sacks.

acellular collagen-fibrin co-gels. Experimentally, we formulated collagen-fibrin co-gels in Teflon ring molds at nine different concentrations and performed tensile tests to failure to obtain material properties of ultimate tensile stress (UTS), tangent modulus, strain energy density, and strain at failure. These experimental results were compared to computational predictions from two hypothetical models for the co-gel: (a) independent, noninteracting networks ("parallel"), and (b) a single network of alternating collagen and fibrin elements ("series").

2 Materials and Methods

2.1 Preparation of Collagen, Fibrin, and Collagen-Fibrin Co-Gels. Collagen gels were formed by reconstituting acid-solubilized rat-tail collagen Type I (Invitrogen, Carlsbad, CA, 5.0 mg/mL) with an alkaline solution consisting of 1M NaOH (Sigma, St. Louis, MO) supplemented with 10× modified Eagle's medium (Sigma), 6% fetal bovine serum (HyClone, Logan, UT), 200 mM L-glutamine (Invitrogen), 0.1% penicillin-streptomycin (Invitrogen), and 250 μg/mL fungizone (Invitrogen). To make fibrin gels, stock solutions of fibrinogen and thrombin were first prepared. Bovine fibrinogen (Sigma) was dissolved in 20 mM HEPES (4-(2-hydroxyethyl)-1-piperazineethanesulfonic acid) buffer saline (Mediatech, Manassas VA; 1 M stock diluted in 0.9% NaCl). A fibrinogen solution was made by mixing 1 part stock fibrinogen with 5 parts 20 mM HEPES buffer saline. A thrombin/Ca^{2+} solution was made by supplementing 1× Dulbecco's modified Eagle's medium (Mediatech) with 2.5% of 25 U/mL thrombin and 0.2% 2N Ca^{2+} (Sigma). Fibrin gels were formed by adding 2 parts fibrinogen solution to 1 part thrombin/Ca^{2+} solution.

Collagen-fibrin co-gels were made at seven different collagen concentrations by adapting the procedure developed in [18], at volumetric proportions of 12.5%, 25%, 37.5%, 50%, 62.5%, 75%, and 87.5% of collagen formulation. Appropriate amounts of each solution corresponding to the target collagen concentration were mixed in the following order: the alkaline solution was first mixed with the thrombin/Ca^{2+} solution, followed by the addition of fibrinogen solution, and last, the addition of the collagen I stock solution. All gel solutions were cast into Teflon annular ring molds (15.5 mm O.D., 11.5 mm I.D.) and incubated overnight at 37 °C. The actual concentrations of collagen and fibrin in the co-gels were determined via biochemical analysis (see the following text), and respective compositions were computed from these results.

2.2 Quantification of Collagen and Fibrin Concentrations. The collagen content in each of the collagen-fibrin co-gels was measured using the hydroxyproline assay [24]. The fibrin content was measured by digesting the collagen-fibrin samples with human plasmin (Sigma) and quantifying the amount of fibrin degradation product using ELISA [25].

2.3 Scanning Electron Microscopy (SEM). Sample preparation for SEM was performed as follows: gels were fixed with 2.5% glutaradehyde (Sigma), followed by post-fixation staining with 1% osmium tetroxide. The samples were sequentially dehydrated in 30%, 50%, 70%, 80%, and 95% ethanol solutions, and freeze-fractured in liquid nitrogen before a final dehydration step in 100% ethanol. The dehydrated gels were further dried using a Tousimis 780A critical point dryer (Tousimis Corp., Rockville, MD) before being mounted on aluminum shims and sputter-coated with platinum for 10 min. High resolution imaging was performed with a Hitachi S-900 field emission gun scanning electron microscope (Hitachi High Technologies America Inc, Pleasanton, CA) at a beam voltage of 2 kV.

2.4 Mechanical Testing. Tensile tests to failure were performed on each gel ring using an Instron 8848 MicroTester (Instron, Norwood, MA) with a 5 N load cell. The rings were mounted over T-bar grips looped through the annulus and were

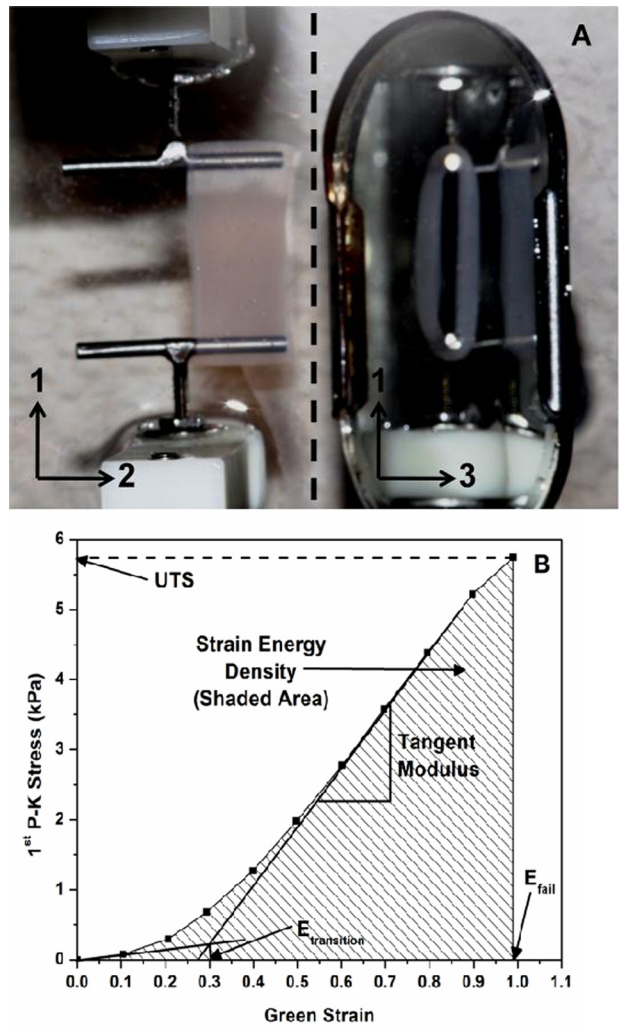

Fig. 1 (*a*) Image showing the mechanical testing setup for collagen-fibrin rings, taken during prestrain. A mirror (to the right of the dotted line) is used to visualize the gel in the 1-3 plane. Dimensions of the gels are measured from these images to calculate the initial area, which is used to convert the force data to 1st Piola-Kirchhoff stress. (*b*) Representative stress-strain plot of a collagen-fibrin co-gel (41% C), showing how each parameter is determined.

submerged in 1 × phosphate buffered saline (Mediatech) throughout the duration of the test (Fig. 1(*a*)). Each ring was initially stretched to a grip-to-grip length of 14.5 mm for 5 s before stretching to failure at a strain rate of 0.13 mm/s. The initial dimensions of the samples were captured using a digital camera during the 5-second prestrain. Force-displacement data were converted to 1st Piola-Kirchhoff Stress (1st PK) versus Green's strain (E) to generate stress-strain curves for each sample. From the stress-strain profiles, the following quantities were computed and compared across the compositions: ultimate tensile stress (UTS), Green strain at failure (E_{fail}), toe-to-linear transition ($E_{transition}$), tangent modulus, and strain energy density (Fig. 1(*b*)). The apparent Poisson's ratio at a stretch ratio of 1.5 was also computed for each co-gel using the following expression [26]:

$$\nu = -\frac{\ln \lambda_2}{\ln \lambda_1} \tag{1}$$

where λ_1 and λ_2 are the stretch ratios in the 1 and 2 directions, respectively, as defined in Fig. 1(*a*). Here, λ_2 was calculated using

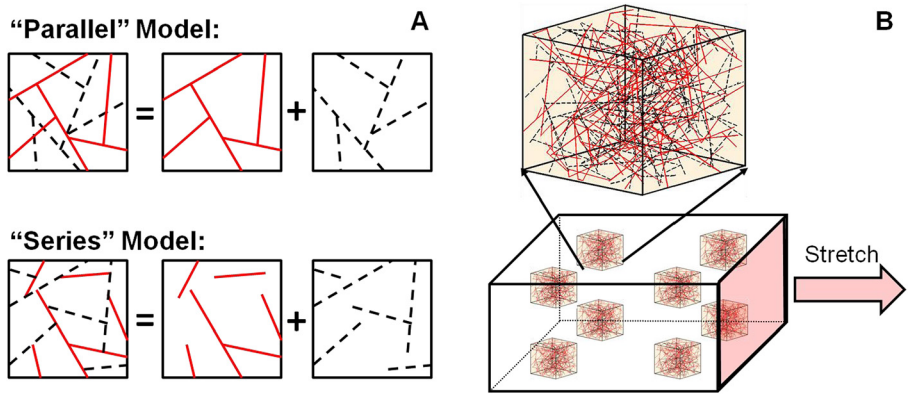

Fig. 2 (*a*) Schematic representation of the parallel and series models of interactions in the two-network cases. (*b*) Model predictions of mechanical behavior in the networks generated using a single finite element with 8 Gauss points; each Gauss point is surrounded by a network RVE.

gel widths in the 2-direction, obtained from digital images taken at test points when $\lambda_1 = 1.0$ (start of test) and $\lambda_1 = 1.5$. The nonlinear expression of Eq. (1) reduces to the standard definition of Poisson's ratio at infinitesimal strain, but remains equal to 0.5 for incompressible materials even at large strain.

2.5 Computational Model. We previously developed a multiscale modeling framework that incorporated a single-component microstructural network to predict the overall mechanical properties of an engineered tissue [27–29]. Briefly, the model couples the macroscopic scale (representing the functional tissue level) with the microscopic scale (representing the fiber network) via volume-averaging. Each Gauss point of the finite element mesh is surrounded by a representative volume element (RVE), which defines the fiber network. Force balances within each RVE are solved instead of a stress-strain constitutive equation. On the microscopic scale, each RVE contains a network of randomly oriented fibrils. A fibril is defined as the straight line segment between two cross-links, and its mechanical behavior is described using an exponential force-strain constitutive relation [30,31]

$$F = \frac{A}{B}\left(\exp\left(BE_f\right) - 1\right) \tag{2}$$

where F is the force on the fiber, and A and B are material constants representing the fiber. The pre-exponential constant A is a measure of the stiffness of the fiber, while B represents the degree of nonlinearity of the fiber. Here, E_f is the fiber Green strain computed from its fiber stretch ratio λ_f

$$E_f = 0.5\left(\lambda_f^2 - 1\right) \tag{3}$$

It should be emphasized that E_f is the Green strain of *individual fibers* in the RVE. As fibers rotate into the direction of stretch, a distribution of fiber Green strains will be obtained, with the largest possible value of E_f corresponding to the macroscopic strain at the gel level, for fibers perfectly oriented in the stretch direction. The average Cauchy stress for each RVE, σ_{ij}, can be shown [28] to be given by

$$\sigma_{ij} = \frac{1}{V}\sum_{\substack{boundary\\ cross-links}} x_i F_j \tag{4}$$

where V is the volume of the RVE, and x_i and F_j are the ith-component of the position and jth-component of the force exerted for each boundary cross-link, respectively. A boundary cross-link is defined whenever a fibril intersects an RVE boundary. To relate the RVE scale to the macroscopic scale, a scale factor x is computed based on the total fiber volume and the fiber volume fraction (see Ref. [28] for the derivation)

$$x = \sqrt{\frac{LA_f}{\theta_0}} \tag{5}$$

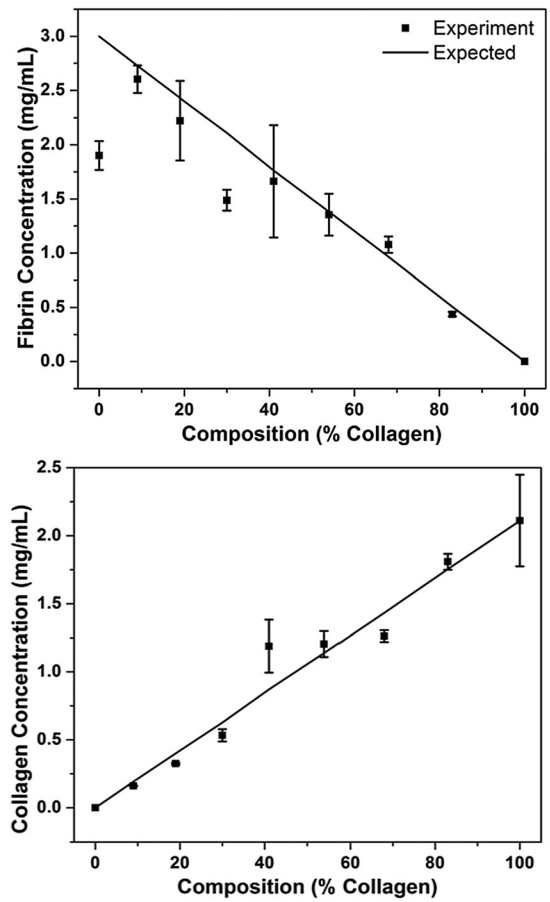

Fig. 3 Results from ELISA and hydroxyproline assays to quantify fibrin and collagen concentrations, respectively, in the gels. In general, no significant loss in either fibrin or collagen is observed in the co-gels. A significant loss in fibrin is observed in the pure fibrin gels; this loss is also macroscopically observed in the gel shrinkage and left-over liquid (containing unaggregated fibrinogen) when removed from the Teflon molds.

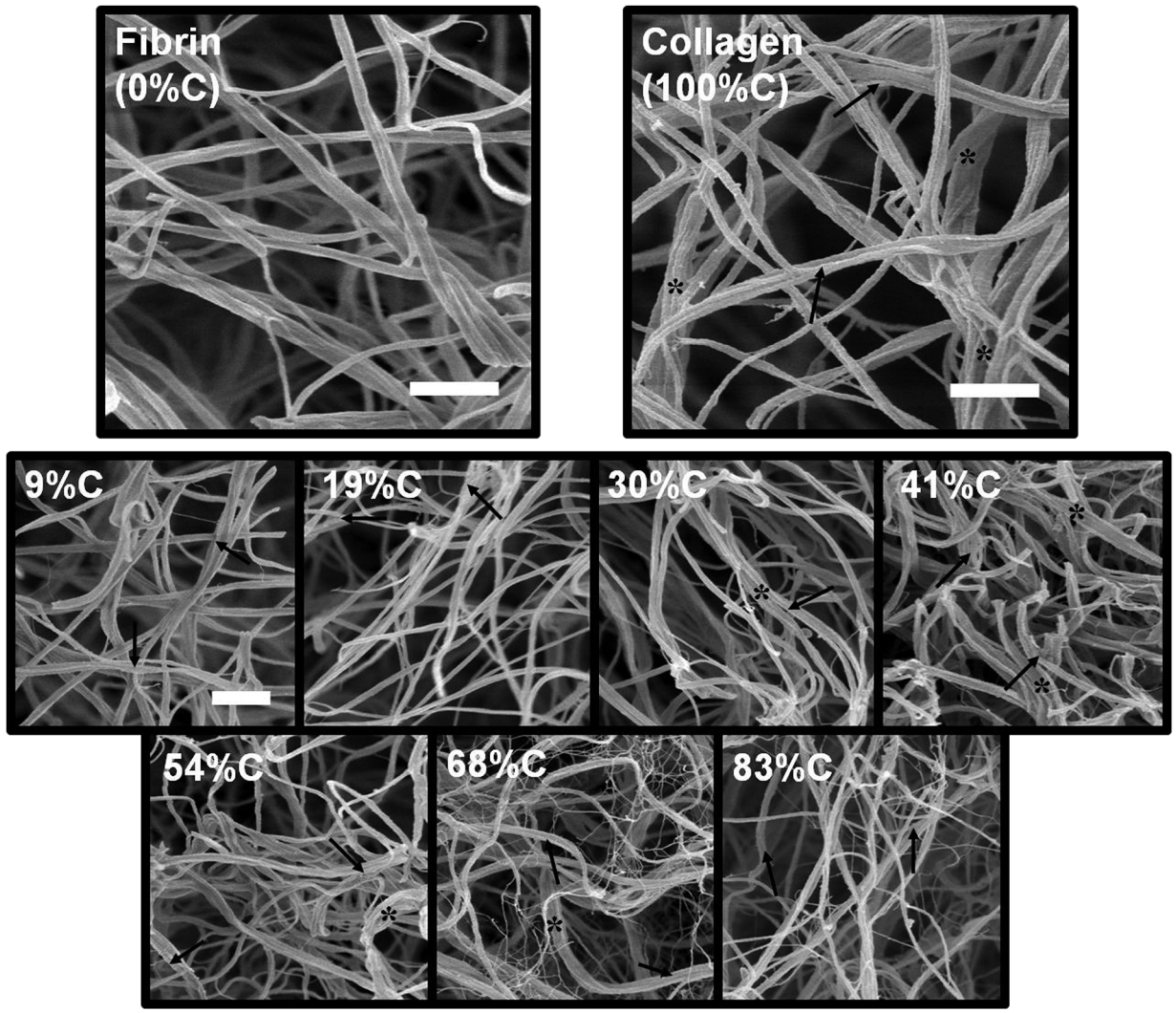

Fig. 4 SEM images taken at 30 000 × of pure fibrin and collagen gels (top) and collagen-fibrin co-gels (bottom). Collagen fibers can be differentiated from fibrin fibers by their characteristic banding pattern (arrows) on and the bundling of (*) the fibers. At higher collagen compositions (68% C, 83% C), wispier, weblike fibrin structures are observed. Scale bars = 1 μm; the scale bar in the 9% C image is representative for all co-gel images.

where the numerator is the total fiber volume given by the product of total fiber length (L) with the fiber cross-sectional area (A_f) and θ_0 is the fiber volume fraction.

The strategy for modeling collagen-fibrin co-gels was as follows. Material constants A and B for collagen and fibrin were first determined by fitting theoretical predictions from our single-network model to the experimental data for pure collagen and fibrin gels. We then modified our algorithm to model a two-network system and considered two different forms of interactions between the two networks (Fig. 2(*a*)).

2.5.1 Parallel Model. For the parallel model, the co-gel was modeled as two distinct, interpenetrating, but not interacting, networks. Two independent networks, one representing each component, were generated for each RVE, the stress was independently calculated for each network, and the sum of the two component stresses was used as the stress of the co-gel. Differences in protein concentration (hence fiber volume fraction θ_0 in Eq. (5)) were modeled by changing the scale factor x between each RVE and the macroscopic scale.

2.5.2 Series Model. In the series model, the co-gel was modeled as a single network with some collagen and some fibrin fibrils. The two-component network was evaluated as a single interconnected network of randomly alternating collagen and fibrin fibrils, by randomly prescribing the respective material constants A and B for collagen and fibrin to each fibril according to the desired compositions. Differences in concentration were modeled by adjusting the fraction of fibrils with each set of properties.

Because the ring test approximates a simple uniaxial extension when, as in our study, the wall thickness of the ring is much smaller than its radius, a single finite element with 8 Gauss points was used to model this simple tensile test (Fig. 2(*b*)), using RVEs containing approximately 700 fibrils each. Model-predicted stress-strain curves were generated by stretching each element to the respective failure strains experimentally observed. The apparent Poisson's ratio was computed in a fashion similar to the experiment, averaged between the 1-2 and 1-3 directions (as defined in Fig. 2(*b*)). Because each network RVE was generated in a random manner, different networks of the same composition gave a slightly different mechanical behavior. For each composition, at least six networks were generated, and the averaged data were computed from the model results.

3 Results

3.1 Biochemical and SEM Results. Figure 3 shows a comparison between the actual fibrin and collagen concentrations in

the gels compared to the expected concentrations calculated from our stock concentrations of fibrinogen and collagen. In general, with the exception of the pure fibrin gels (0% C), there was good agreement between the actual and expected fibrin and collagen concentrations, which indicates no significant loss of either protein in the co-gels during the casting process. The difference between the expected fibrin concentration (3 mg/mL) and the actual concentration (1.9 mg/mL) in the pure fibrin gels was also usually observed, where there was significant liquid loss and gel shrinkage when the pure fibrin gel samples were removed from the Teflon molds. This protein loss was due to unaggregated fibrinogen left in the liquid. From these experimental data, the compositions of the 7 co-gels were calculated to be 9%, 19%, 30%, 41%, 54%, 68%, and 83% collagen, respectively. An expected linear decrease in the total protein concentration with increasing collagen content was observed, since the co-gels were made by mixing volumetric proportions of 2.1 mg/mL collagen formulation with 3.0 mg/mL fibrin formulation.

The SEM images of the fibrin and collagen gels (Fig. 4) showed a similar network microstructure between the pure networks, with fibril diameters on the order of 100 nm. Characteristic banding patterns of collagen fibrils can be observed in the collagen images (marked with arrows), and the bundling of fibrils (marked with an asterisk) to form thicker collagen fibers. These two characteristics of the collagen network, absent in the fibrin network, allow identification of collagen fibrils in the co-gels. It should be emphasized that while bundled and/or banded fibrils are collagen, the unbanded, unbundled fibrils could belong to either network. From the co-gel images, composite fiber networks comprised of interpenetrating collagen and fibrin fibrils can be seen, with more banded and bundled fibrils observed with increasing collagen composition. At high collagen compositions (68% C and 83% C), a fine network of wispy fibers is observed to form around the thicker fibrils. Most of the thicker fibrils at these compositions appear to be banded, indicating that they are collagen; furthermore, fibrin is known to form such wispy structures depending on the gelation conditions [32]. Hence, the fine network seen at higher collagen compositions is likely to be fibrin. Collectively, these images confirm that a composite network of collagen and fibrin fibrils is formed in our co-gels; however, it should be noted that no inference on the *nature of interactions* between collagen and fibrin can be made from these images.

3.2 Mechanical Property Results. Using the protein concentrations of the pure gels determined experimentally (1.9 mg/mL for fibrin; 2.1 mg/mL for collagen) and a fibril diameter of 100 nm for both fibrin and collagen, as observed from the SEM images, the single-network model was fitted to the experimental data to obtain material parameters A and B for idealized fibrin and collagen fibers (Fig. 5). The relative linearity of the stress-strain curve for fibrin is reflected in the small fitted B value. This fit suggests that the mechanical behavior of fibrin fibrils is largely linear; a small toe region in the overall stress-strain curve is still observed, however, which arises from the reorganization and rotation of the fibrils as the gel is stretched. That collagen is a much stiffer fiber than fibrin (hence, a larger A value) is reflected in the similar stress scales for both fibers but much lower strain range for collagen.

Using these fitted parameters for fibrin and collagen, model predictions for the tensile behavior at the seven intermediate compositions were made using the parallel and series models of interactions as previously explained (Fig. 6) and compared to the sample averaged stress-strain curves from experiment. At all compositions, the model elements were stretched to the respective experimental strains at failure (Fig. 7(*a*)) to simulate the experiments. Dotted lines for the parallel model in Fig. 6 represent hypothetical model stress-strain behavior beyond the failure strain of a pure collagen network. These regions are physically unrealistic, since the collagen network in such a parallel network system

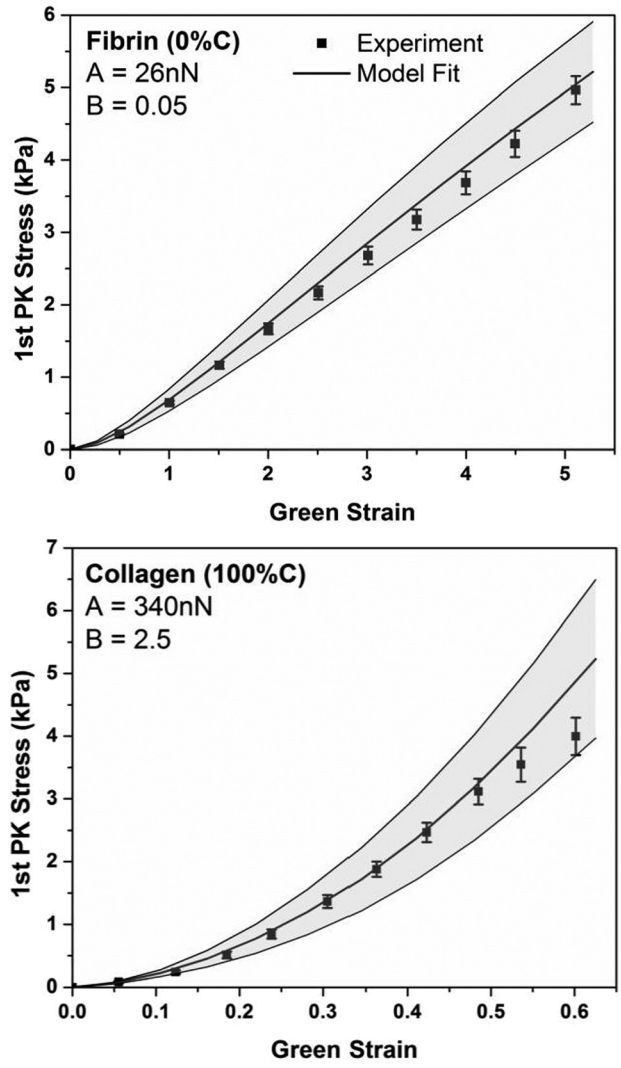

Fig. 5 Model fits to the experimental data to obtain material parameters *A* and *B* for fibrin and collagen, respectively. Collagen shows a much higher stiffness (in the *A* value) and a larger degree of nonlinearity (the *B* value) than fibrin. Error bars on the experimental data represent 95% CI, n $\geq$ 7 for both collagen and fibrin. Error bands on the model fits represent 95% CI, generated from four different networks for each.

would fail and could not continue to carry the load. Across all of the compositions, the experimental curves were found to fall between or within the two models, with the parallel model providing the upper bound, and the series model providing the lower bound. At the lowest collagen co-gel concentration (9% C), the series model appears to capture the tensile behavior of the composite network well. A transition towards the parallel model occurs with increasing collagen content, such that a good agreement between the parallel model and experimental data was observed at high collagen concentrations of 68% C and 83% C.

A comparison of the material properties of the co-gels across compositions extracted from the experimental data is provided in Fig. 7. In terms of failure behavior, a rapid decrease in strain at failure is observed as the collagen content increases (Fig. 7(*a*)), while the UTS of the co-gels remain relatively constant across the compositions (Fig. 7(*b*)). Accordingly, the strain energy density (Fig. 7(*c*)) decreases while the tangent modulus (Fig. 7(*d*)) increases with increasing collagen composition. Similar to observations from the stress-strain curves, the experimental data for the strain energy density, the UTS, and tangent modulus were found to be bracketed by the parallel and series model predictions.

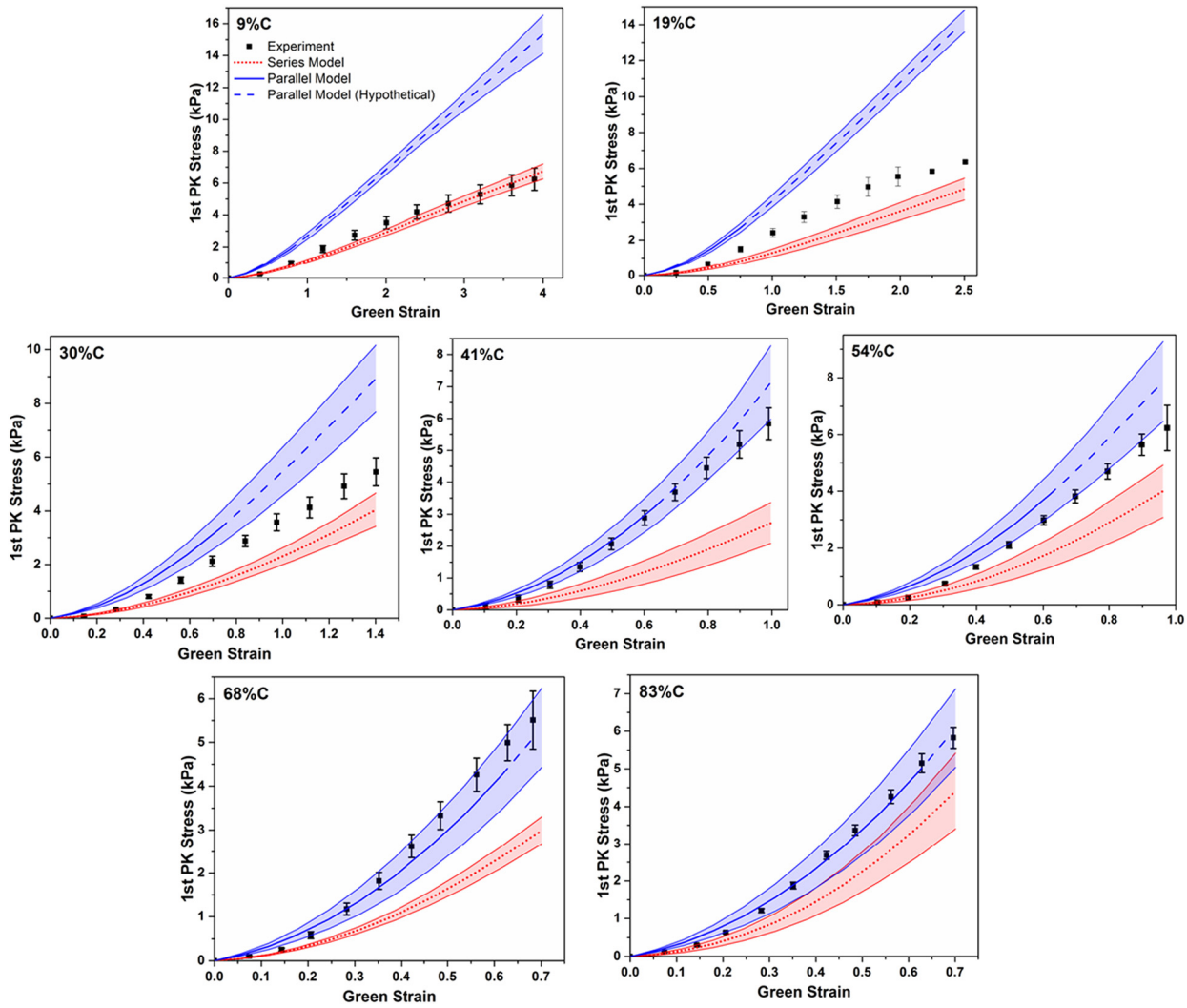

Fig. 6 Model predictions from the parallel and series models compared with experiment (■) across all seven compositions of the co-gels. In the parallel model, the dashed lines represent hypothetical stress-strain regions after the failure strain of pure collagen, above which the collagen network is expected to have catastrophically failed. In all cases, the parallel and series models provide upper and lower bounds to the experimental data. The series model shows better agreement to the experiment at low collagen content (9% C), while the parallel model shows better agreement at high collagen contents (68% C and 83% C). Error bars represent 95% CI; n $\geq$ 5 gels for experiments, n $\geq$ 6 networks for models.

Transition strain (Fig. 7(*e*)) can be considered as an estimate of the amount of strain needed for the fibrils to reorganize, rotate, and straighten into the direction of stretch. While both the parallel and series models over-predict this transition strain, they are able to capture the general trend of decreasing transition strain with increasing collagen composition (Fig. 7(*e*)). Experimentally, the apparent Poisson's ratio (Fig. 7(*f*)) exhibited an increasing trend from 0.6 to 1.5 as the collagen content increased from 0% to 100% (p value < 0.05 for the null hypothesis that the slope of the linear regression equals zero). While the same regression analysis performed on both parallel and series models predicted constant apparent Poisson's ratios (i.e., $p > 0.05$ in both cases, such that the null hypothesis could not be rejected at the 95% confidence level) across all compositions, the values were of a similar order of magnitude to the experimental data.

4 Discussion

An analysis of the experimental data coupled with model predictions provides insight into how mechanical properties change with composition and the forms of interactions that exist between fibrin and collagen in these co-gels. That fibrin is a very compliant biomaterial is well documented [33,34], and our results are consistent with these findings that fibrin networks can have extensibilities beyond 200%. The addition of collagen to fibrin led to intermediate mechanical properties (strain at failure, UTS, tangent modulus); nonlinear trends with increasing collagen concentration showed that these properties could not be predicted by the simple rule of mixtures. As the collagen content increased, the macroscopic stiffness of the gel increased at the expense of the extensibility; however, failure was observed at strains well beyond the failure strain of pure collagen, an effect especially pronounced at low collagen concentrations. The lack of an abrupt transition in properties indicates that plastic failure of the stiffer collagen network did not occur in the co-gels. Additional experiments on 41% C co-gels, in which the gels were first prestretched to the failure strain of pure collagen, showed statistically similar failure properties (UTS, strain at failure) to gels that were not prestretched, with a small effect ($\sim$15%) on the tangent modulus (data not shown). These results further confirm the absence of plastic failure in the stiffer collagen network. Collectively, these results suggest that the co-gels were not dominated solely by either network, but rather that complex interactions between the networks gave rise to

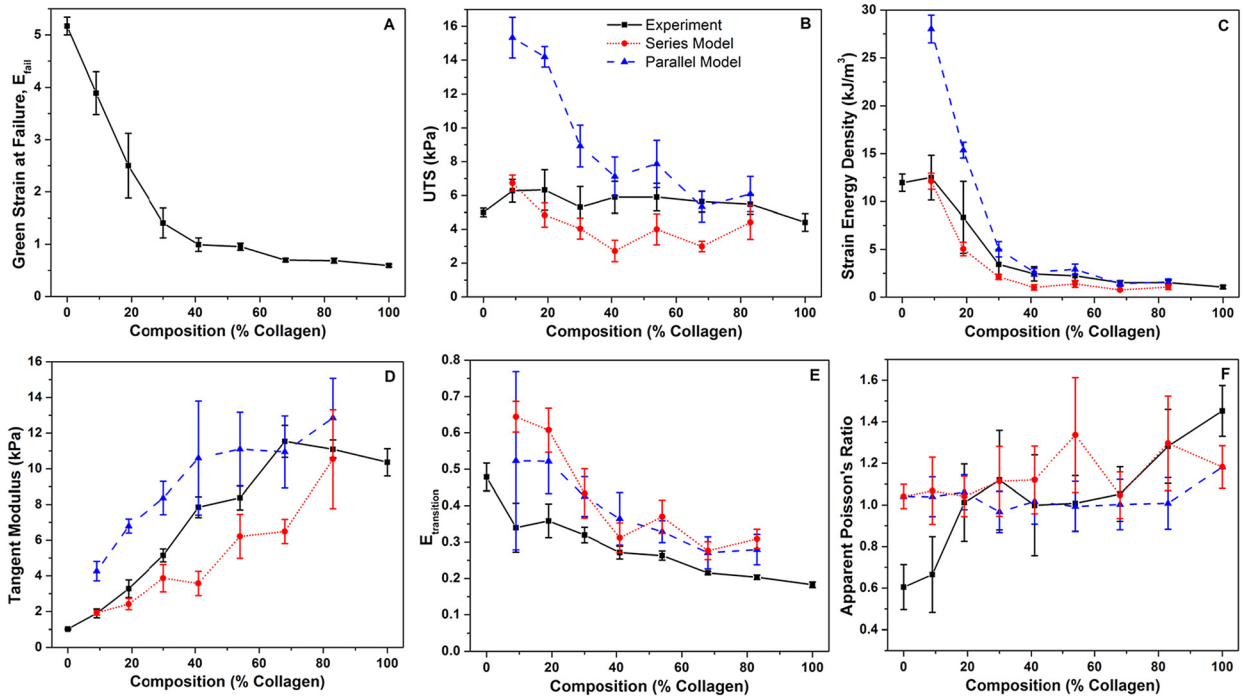

Fig. 7 Material properties of co-gels from the experiment (■, solid lines) compared with model predictions from the parallel (▲, dashed lines) and series (•, dotted lines) models. Parallel models reflect properties in the hypothetical region (defined in Fig. 6) beyond the failure strain of collagen. In general, both models are able to predict trends in the strain energy density, tangent modulus, and transition strain. The experimental data is bracketed by the parallel and series models in the UTS, strain energy density, and tangent modulus. Models predict the apparent Poisson's ratio on the same order of magnitude as the experiment. Error bars represent 95% CI; n ≥ 5 gels for experiments, n ≥ 6 networks for models.

intermediate properties. Complementary contributions to the overall mechanical behavior by both networks occur in the co-gels: the fibrin network gives extensibility by bearing stretch, while the collagen network provides stiffness by bearing load.

Across all compositions, the collagen-fibrin co-gels exhibited large apparent Poisson's ratios above the incompressibility limit. Since these gels are largely composed of water (>99 vol. %), it is not surprising that significant shrinkage occurs during stretch, where liquid is squeezed out of the gel between the fibrils as they rotate into the direction of stretch [35]. While an increase in the apparent Poisson's ratio with increasing collagen composition is observed, it is unclear whether this effect is due to a decrease in fibril density with increasing collagen content in our co-gels, or fibrin is better able to retain water within its network. Similarly, it is unclear whether the decrease in the transition strain with increasing collagen content is due to rotational hindrances from higher fibril densities, or an inherent nonlinear behavior of the respective networks.

The conventional preparation techniques for SEM used in this study has been shown to introduce artifacts in the microstructure compared with cryo-SEM preparation techniques, such as substantial shrinkage of the sample resulting in smaller fibril diameters and smaller void spaces [36], and collapse and clumping of fibrils [37]. Nevertheless, our SEM images provide important information on the overall morphology of the co-gels at different concentrations, showing co-existing networks of collagen and fibrin in co-gels, along with changes in the fibrin network architecture at higher collagen concentrations. An average fibril diameter of 100 nm, based on our SEM images, was used as input into our model to relate the RVE to the macroscopic scale in Eq. (5). While a different fibril diameter would quantitatively change the fitted material parameters A and B for collagen and fibrin, the key qualitative results from these model fits remain unchanged: that collagen is stiffer (larger A value) and exhibits a greater degree of nonlinearity (larger B value) than fibrin. The effect of fibril diameter is fully subsumed in the alteration of A and B parameters; subsequent model predictions using these altered parameters will give the same qualitative and quantitative results as presented in this paper.

The parallel and series models presented here were meant as gross idealizations of interactions and were not intended to describe actual interactions in our co-gels. However, a comparison of our simulations with the experimental data provides some insight. Figure 8 illustrates the differences in fibril stretch and fibril force distributions between the parallel and series models. In the parallel model, both networks experience equal stretches (Fig. 8(*a*)), while the overall load is unevenly distributed between the networks according to their relative properties; hence, in this model, the overall mechanical behavior is largely dominated by the stiffer collagen network (Fig. 8(*b*)). This phenomenon is demonstrated by the uncharacteristically high stresses observed when the parallel two-fiber networks are stretched beyond the failure strain of pure collagen at low collagen content (9% C) in the hypothetical region (Figs. 6 and 7(*b*)). In the series model, the macroscopic strain is disproportionately distributed among the two fibril populations according to their relative stiffness (Fig. 8(*c*)), while the overall load is borne equally by fibrils from both networks (Fig. 8(*d*)). While we are unable to observe definitively parallel-like or series-like interactions between collagen and fibrin fibrils from our SEM images, inferences can be made from the comparison of our model predictions with the experimental data. At low collagen content, close agreement between the experimental data and the series model suggests that the sparse collagen fibrils do not form a percolating collagen network, however, are dispersed among a fibrin-dominant network, i.e., "islands" of collagen fibrils are present in a series-like manner with the extensive fibrin matrix. While these sparse collagen structures contribute to the overall gel stiffness, they bear a lower proportion of the strain such that macroscopically, the gel can be strained beyond the failure strain of pure collagen; the

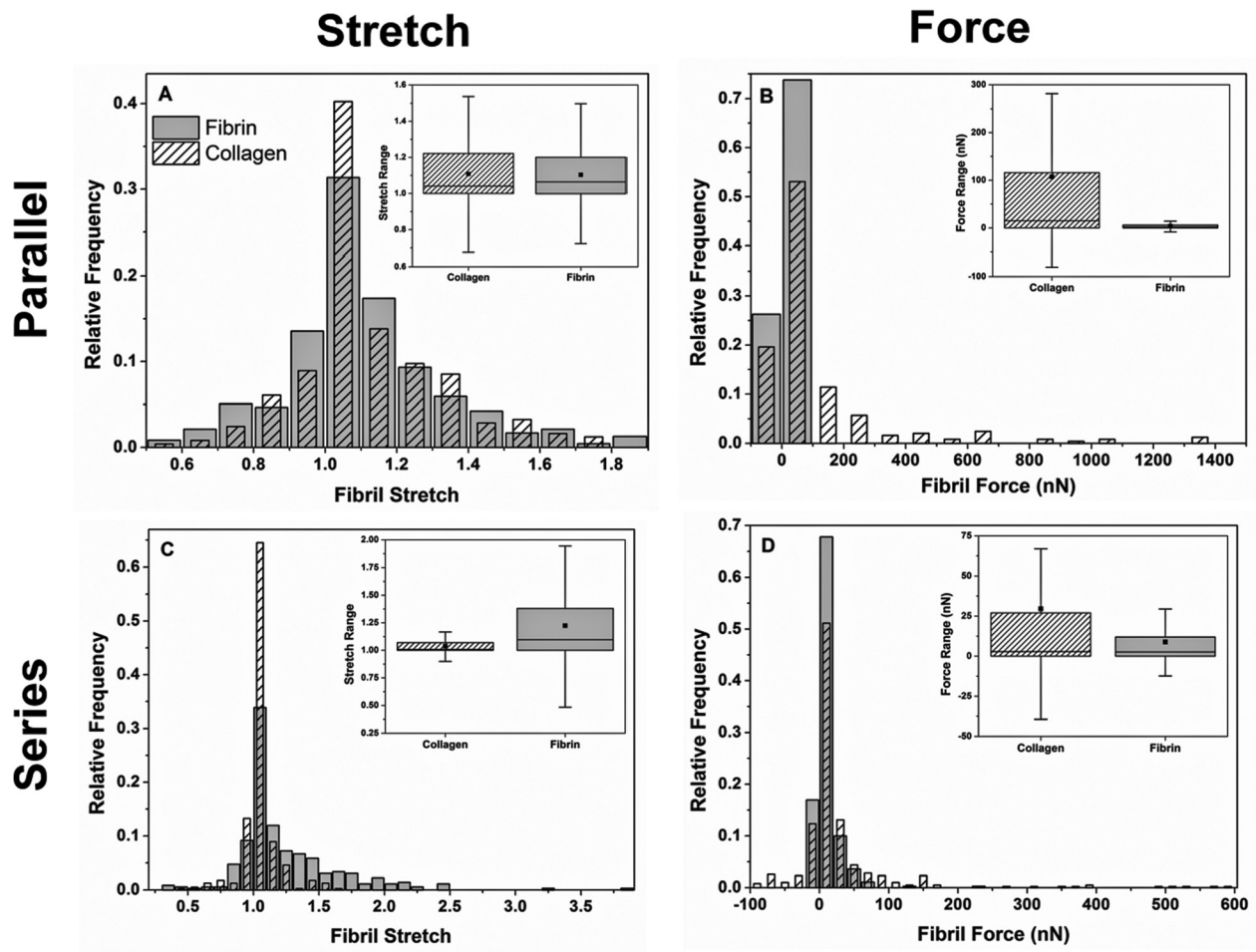

Fig. 8 Fibril stretch and fibril force distributions in the parallel and series models after the macroscopic stretch. In the parallel model, the collagen and fibrin networks exhibit similar fibril stretch distributions, however, forces in the collagen fibrils are much larger than those in the fibrin fibrils. In the series model, a much smaller difference between the collagen and fibrin fibril force distributions is observed, however, fibrin fibrils bear a larger proportion of macroscopic stretch. Distributions are of 54% C networks, taken from an RVE at a Gauss point after the final stretch step. The ■ in the box plots represent the distribution mean and whiskers represent outliers within the interquartile range.

macroscopic strain of the gel is dominated by the fibrin network. At a high collagen content (68% C and 84% C), the parallel model provides a good fit to the experimental data, suggesting a collagen-dominated network. In these cases, where the gel is largely composed of the stiffer collagen network, the strain is dictated by this stiffer matrix. The overall mechanical behavior appears additive in a parallel-like fashion, where the smaller contribution to load-bearing by fibrin adds to that of the stiffer collagen network. In addition, the failure strain is largely dictated by the extensive collagen network, while the slight increase in the experimental failure strain may be attributed to sparsely distributed fibrin fibrils associated with the collagen network. At intermediate compositions, the parallel and series models provide bounds for the experimental data, which suggest a mixture of such interactions. Conceivably, both collagen and fibrin form respective independent interconnected networks in a parallel fashion, however, individual fibrils from each network can be associated with each other across the networks, forming series connections. In addition, more inter-fibril mechanical connections may be formed as the gel is stretched and as fibrils from each network rotate and reorganize with each other. While our results strongly indicate interactions between collagen and fibrin, it remains unclear whether these interactions are chemical (i.e., chemical bonds between fibrils) or mechanical (physically entangled fibrils) in nature. Work is in progress to understand the nature of these interactions by the digestion of either network in the co-gels.

Previous studies on collagen-fibrin co-gels have focused on cellular responses (gel compaction and cell proliferation) on collagen-fibrin scaffolds of different compositions and concentrations for applications in cardiovascular tissue engineering [18,19]. Our work expands on these studies by exploring the fundamental structure-function-composition relationships in these collagen-fibrin composite networks, allowing for a better understanding of the mechanical environments that cells experience in such tissue-engineered constructs. In addition, a progression in composition occurs in our tissue-engineered media equivalents (MEs): with cells initially seeded in a fibrin gel, the MEs undergo compositional changes during the growth and remodeling process, transitioning from a pure fibrin-based construct at casting to a largely collagen-based construct after weeks of culture [38]. That the cells in our MEs experience changes in the mechanical environment throughout the remodeling process may have implications on the cellular responses elicited at different stages of growth and remodeling.

One of the key goals in tissue engineering is to design tissue equivalents with mechanical properties comparable to the native tissues. Efforts towards this goal have included modifying or manipulating the ECM content, such as stimulating the production of collagen to improve tissue strength and stiffness [5], or directly incorporating elastin to confer tissue compliance [2]. While tissue engineers understand the importance of different ECM components towards the overall mechanical behavior and function,

our work emphasizes the *complexity of interactions* between multiple ECM components in conferring mechanical properties. This work is a step forward towards better understanding the complexities of how tissues behave mechanically, due to the presence of various components within the tissue, allowing for more rational designs for bioengineered tissues. In addition, a vast majority of multicomponent models of native tissue mechanics (e.g., Refs. [39,40]) rely on parallel-type interactions, adding up contributions from the different components. Our results for the collagen-fibrin model system strongly suggest that alternative approaches may be needed for some tissues.

5 Conclusions

This current work offers new insights into how collagen and fibrin fibril networks interact with each other, and furthers the understanding of fundamental structure-composition-function relationships in collagen-fibrin co-gels. A comparison of the model results with the experiments suggests complex interactions between collagen and fibrin networks that vary with composition, with a series model being better for collagen-poor gels and a parallel model being better for collagen-rich gels. This study demonstrates that purely parallel (i.e., additive) models may not be adequate to describe tissue mechanics.

Acknowledgment

The authors gratefully acknowledge financial support from the National Institutes of Health (Grant No. R01-EB005813) and the American Heart Association (Grant No. 11PRE5410003). We thank Sandy Johnson for her help with biochemical analysis. Parts of this work were carried out in the Characterization Facility, University of Minnesota, which receives partial support from the NSF through the MRSEC program.

References

[1] Lee, C. H., and Singla, A. and Lee, Y., 2001, "Biomedical Applications of Collagen," Int. J. Pharm., **221**(1-2), pp. 1–22.
[2] Buttafoco, L., Kolkman, N. G., Engbers-Buijtenhuijs, P., Poot, A. A., Dijkstra, P. J., Vermes, I., and Feijen, J., 2006, "Electrospinning of Collagen and Elastin for Tissue Engineering Applications," Biomaterials, **27**(5), pp. 724–734.
[3] Couet, F., Rajan, N., and Mantovani D., 2007, "Macromolecular Biomaterials for Scaffold-Based Vascular Tissue Engineering," Macromol. Biosci., **7**(5), pp. 701–718.
[4] Mol, A., van Lieshout, M. I., Dam-de Veen, C. G., Neuenschwander, S., Hoerstrup, S. P., Baaijens, F.P.T., and Bouten, C.V.C., 2005, "Fibrin as a Cell Carrier in Cardiovascular Tissue Engineering Applications," Biomaterials, **26**(16), pp. 3113–3121.
[5] Grassl, E. D., Oegema, T. R., and Tranquillo, R. T., 2003, "A Fibrin-Based Arterial Media Equivalent," J. Biomed. Mater. Res. Part A, **66A**(3), pp. 550–561.
[6] Grassl, E. D., Oegema, T. R., and Tranquillo, R. T., 2002, "Fibrin as an Alternative Biopolymer to Type-I Collagen for the Fabrication of a Media Equivalent," J. Biomed. Mater. Res., **60**(4), pp. 607–612.
[7] Mosesson, M. W., 2005, "Fibrinogen and Fibrin Structure and Functions," J. Thromb. Haemost., **3**(8), pp. 1894–1904.
[8] Blombäck, B. and Bark, N., 2004, "Fibrinopeptides and Fibrin Gel Structure," Biophys. Chem., **112**(2-3), pp. 147–151.
[9] Mosesson, M. W., 2004, "John Ferry and the Mechanical Properties of Cross-Linked Fibrin," Biophys. Chem., **112**(2-3), pp. 215–218.
[10] Roska, F. J., and Ferry J. D., 1982, "Studies of Fibrin Film. I. Stress Relaxation and Birefringence," Biopolymers, **21**(9), pp. 1811–1832.
[11] Roska, F. J., Ferry, J. D., Lin, J. S., and Anderegg, J. W., 1982, "Studies of Fibrin Film. II. Small-Angle X-Ray Scattering," Biopolymers, **21**(9), pp. 1833–1845.
[12] Whittaker, P. and Przyklenk, K., 2009, "Fibrin Architecture in Clots: A Quantitative Polarized Light Microscopy Analysis," Blood Cells Mol. Dis., **42**(1), pp. 51–56.
[13] Miller, E. J., 1984, "Chemistry of the Collagens and Their Distribution," *Extracellular Matrix Biochemistry*, Elsevier, New York, pp. 41–81.
[14] Christiansen, D. L., Huang, E. K., and Silver, F. H., 2000, "Assembly of Type I Collagen: Fusion of Fibril Subunits and the Influence of Fibril Diameter on Mechanical Properties," Matrix Biol., **19**(5), pp. 409–420.
[15] Eyre, D. R., Paz, M. A., and Gallop, P. M., 1984, "Cross-Linking in Collagen and Elastin," Annu. Rev. Biochem., **53**(1), pp. 717–748.
[16] Eppell, S. J., Smith, B. N., Kahn, H., and Ballarini, R., 2006, "Nano Measurements With Micro-Devices: Mechanical Properties of Hydrated Collagen Fibrils," J. R. Soc., Interface, **3**(6), pp. 117–121.
[17] Wagenseil, J. E., Wakatsuki, T., Okamoto, R. J., Zahalak, G. I., and Elson, E. L., 2003, "One-Dimensional Viscoelastic Behavior of Fibroblast Populated Collagen Matrices," J. Biomech. Eng., **125**(5), pp. 719–725.
[18] Cummings, C. L., Gawlitta, D., Nerem, R. M., and Stegemann, J. P., 2004, "Properties of Engineered Vascular Constructs Made From Collagen, Fibrin, and Collagen-Fibrin Mixtures," Biomaterials, **25**(17), pp. 3699–3706.
[19] Rowe, S. L. and Stegemann, J. P., 2006, "Interpenetrating Collagen-Fibrin Composite Matrices with Varying Protein Contents and Ratios," Biomacromolecules, **7**(11), pp. 2942–2948.
[20] Rowe, S. L. and Stegemann, J. P., 2009, "Microstructure and Mechanics of Collagen-Fibrin Matrices Polymerized Using Ancrod Snake Venom Enzyme," J. Biomech. Eng., **131**(6), p. 061012.
[21] Duckert, F. and Nyman, D., 1978, "Factor XIII, Fibrin and Collagen," Suppl. Thromb. Haemost., **63**, pp. 391–396.
[22] Mosher, D. F. and Schad, P. E., 1979, "Cross-Linking of Fibronectin to Collagen by Blood Coagulation Factor XIIIa," J. Clin. Invest., **64**(3), pp. 781–787.
[23] Stemberger, A., Jilek, F., Hormann, H., and Blumel, G., 1977, "Fibrinogen-Collagen Interactions," Thromb. Haemost., **38**, p. 305.
[24] Stegemann, H. and Stalder, K., 1967, "Determination of Hydroxyproline," Clin. Chim. Acta, **18**(2), pp. 267–273.
[25] Ahmann, K. A., Weinbaum, J. S., Johnson, S. L., and Tranquillo, R. T., 2010, "Fibrin Degradation Enhances Vascular Smooth Muscle Cell Proliferation and Matrix Deposition in Fibrin-Based Tissue Constructs Fabricated *in vitro*," Tissue Eng., **16**(10), pp. 3261–3270.
[26] Lake, S. P. and Barocas, V. H., 2011, "Mechanical and Structural Contribution of Non-Fibrillar Matrix in Uniaxial Tension: A Collagen-Agarose Co-Gel Model," Ann. Biomed. Eng., **39**(7), pp. 1891–1903.
[27] Chandran, P. L. and Barocas, V. H., 2007, "Deterministic Material-Based Averaging Theory Model of Collagen Gel Micromechanics," J. Biomech. Eng., **129**(2), pp. 137–147.
[28] Stylianopoulos, T. and Barocas, V. H., 2007, "Volume-Averaging Theory for the Study of the Mechanics of Collagen Networks," Comput. Method Appl. M., **196**(31-32), pp. 2981–2990.
[29] Sander, E. A., Stylianopoulos, T., Tranquillo, R. T., and Barocas, V. H., 2009, "Image-Based Multiscale Modeling Predicts Tissue-Level and Network-Level Fiber Reorganization in Stretched Cell-Compacted Collagen Gels," Proc. Natl. Acad. Sci., **106**(42), pp. 17675–17680.
[30] Fung, Y.-C., 1993, *Biomechanics: Mechanical Properties of Living Tissues* Springer, New York.
[31] Billiar, K. L. and Sacks, M. S., 2000, "Biaxial Mechanical Properties of the Native and Glutaraldehyde-Treated Aortic Valve Cusp: Part II—A Structural Constitutive Model," J. Biomech. Eng., **122**(4), pp. 327–335.
[32] Rowe, S. L., Lee, S. Y., and Stegemann, J. P., 2007, "Influence of Thrombin Concentration on the Mechanical and Morphological Properties of Cell-Seeded Fibrin Hydrogels," Acta Biomater., **3**(1), pp. 59–67.
[33] Guthold, M., Liu, W., Sparks, E. A., Jawerth, L. M., Peng, L., Falvo, M., Superfine, R., Hantgan, R. R., and Lord, S. T., 2007, "A Comparison of the Mechanical and Structural Properties of Fibrin Fibers with Other Protein Fibers," Cell Biochem. Biophys., **49**(3), pp. 165–181.
[34] Liu, W., Jawerth, L. M., Sparks, E. A., Falvo, M. R., Hantgan, R. R., Superfine, R., Lord, S. T., and Guthold, M., 2006, "Fibrin Fibers Have Extraordinary Extensibility and Elasticity," Science, **313**(5787), p. 634.
[35] Tower, T. T., Neidert, M. R., and Tranquillo, R. T., 2002, "Fiber Alignment Imaging During Mechanical Testing of Soft Tissues," Ann. Biomed. Eng., **30**(10), pp. 1221–1233.
[36] Stuart, K. and Panitch, A., 2008, "Influence of Chondroitin Sulfate on Collagen Gel Structure and Mechanical Properties at Physiologically Relevant Levels," Biopolymers, **89**(10), pp. 841–51.
[37] Lewis, J. L., Johnson, S. L., Oegema, T. R., 2002, "Interfibrillar Collagen Bonding Exists in Matrix Produced by Chondrocytes in Culture: Evidence by Electron Microscopy," Tissue Eng., **8**, pp. 989–995.
[38] Syedain, Z. H., Weinberg, J. S., and Tranquillo, R. T., 2008, "Cyclic Distension of Fibrin-Based Tissue Constructs: Evidence of Adaptation During Growth of Engineered Connective Tissue," Proc. Natl. Acad. Sci., **105**(18), pp. 6537–6542.
[39] Alford, P. W., Humphrey, J. D., and Taber, L. A., 2007, "Growth and Remodeling in a Thick-Walled Artery Model: Effects of Spatial Variations in Wall Constituents," Biomech. Model Mechanobiol., **7**, pp. 245–262.
[40] Stylianopoulos, T. and Barocas, V. H., 2007, "Multiscale, Structure-Based Modeling for the Elastic Mechanical Behavior of Arterial Walls," J. Biomech. Eng., **129**(4), pp. 611–618.